Renewable Energy 96 (2016) 190–202

Contents lists available at ScienceDirect

Renewable Energy

journal homepage: www.elsevier.com/locate/renene

The effect of the physical boundary conditions on the thermal performance of molten salt thermocline tank

Zheshao Chang [a, b], Xin Li [a, *], Chao Xu [c], Chun Chang [a], Zhifeng Wang [a], Qiangqiang Zhang [a], Zhirong Liao [a], Qing Li [a]

[a] Key Laboratory of Solar Thermal Energy and Photovoltaic System, Institute of Electrical Engineering, Chinese Academy of Sciences, Beijing, 100190, China
[b] University of Chinese Academy of Sciences, Beijing, 100049, China
[c] North China Electric Power University, Beijing, 100190, China

ARTICLE INFO

Article history:
Received 5 October 2015
Received in revised form
21 March 2016
Accepted 19 April 2016
Available online 4 May 2016

Keywords:
Thermocline
Molten salt
Insert liner
Truncated cone shaped tank
Thermal performance
Entropy generation

ABSTRACT

Methods of solving some of the critical design consideration associated with the thermocline storage system with unusual physical boundary conditions bring new problems: the effect of insert liner should not be ignored with small solid filler size, and it is hard to take advantage of truncated cone shaped tank for decreasing the potential of thermal ratcheting and increasing the maximum height of the tank, both while maintaining a good efficiency.

In this study, a transient two-dimensional and two-temperature model is developed to investigate the heat transfer and fluid dynamics in a molten salt thermocline thermal storage system. After model validation, the effects of physical boundary conditions including insert liner and sloped wall on the thermal performance of thermocline storage system is investigated through the entropy generation analysis.

The results show that both of the axial and radial convex size of the liner should be as small as possible, resulting in smaller average velocity and less disturbance in the flow. The truncated cone shaped tank has an advantage in the charging process with low entropy generation in molten salt and solid material, while it goes against the discharging process. It is found that larger inclined angle of the sloped wall causes smaller thermocline thickness and entropy generation with the same tank height and tank volume for truncated cone shaped tanks. Besides, larger tank height is better for the truncated cone shaped tanks with the same tank volume.

1. Introduction

Among the various utility scale renewable energy technologies, concentrated solar power (CSP) has been identified as a promising and emerging renewable energy technology with the ability to store energy as high temperature heat and continue producing power when solar energy is not available. The integration of solar thermal energy storage (TES) is a viable means to enhance dispatchability, increase the value of concentrated solar energy and make the plant more reliable.

A number of viable candidates for TES systems that might be applied on a commercial scale for CSP plants have been investigated in the literature, usually including three types: sensible, latent and thermochemical, among which sensible heat storage has tremendous preponderance over other thermal storage mechanisms due to its low cost and design simplicity.

Sensible heat storage using molten salt as the storage medium and direct heat transfer fluid can offer the best balance of capacity, cost, efficiency and usability at high temperatures [1], so molten salt sensible heat TES system are widely applied presently [2], especially the two-tank system.

The two-tank system has a high-temperature tank and a low-temperature tank for storing molten salt. It is the most mature utility-scale thermal energy storage (TES) system for CSP plants, and has been applied or projected in many CSP plants. However, the two-tank molten salt TES system has very limited space for cost reduction.

The single-tank thermocline (STTC) TES system has only one storage tank and would use molten salt as the direct heat transfer fluid, storing energy gathered in the solar field, and transferring

* Corresponding author.
E-mail address: drlixin@mail.iee.ac.cn (X. Li).

http://dx.doi.org/10.1016/j.renene.2016.04.043
0960-1481/

Nomenclature

a, b, c, d	axial and radial size of the insert liner, m
C_p	specific heat capacity, J/kg K
D	diameter of the tank, m
$\vec{e_r}, \vec{e_x}$	unit vector in the r and x direction, respectively
Ex	exergy, W
F	inertial coefficient
g	acceleration due to gravity, m/s^2
H	tank height, m
h_i	interstitial heat transfer coefficient, W/m^3 K
K	permeability of porous material, m^2
k	thermal conductivity, W/m K
l	length, m
$\dot{m}$	mass flow rate, kg/s
Nu	Nusselt number
P	thermal power, W
p	pressure, Pa
Pr	Prandtl number
Q	heat, J
Re	Reynolds number
$\dot{S}'''$	Entropy generation rate per unit volume, W/m^3 K
T	temperature, K
t	time, s
v	velocity, m/s

Greek symbols

ε	porosity of packed-bed region
η	efficiency
μ	viscosity, kg/m s
ρ	density, kg/m^3

Subscripts

Air	air
crit	critical value
c	cold fluid
dc	discharging
eff	effective value
gen,l	liquid entropy generation
gen,s	solid entropy generation
h	hot fluid
i	insulation layers or tank steel
in	inlet
l	length, liquid material
out	outlet
s	solid material
st	steel wall
store	energy stored

that energy when needed. With the hot and cold fluid in a single tank, the thermocline storage system relies on thermal buoyancy to maintain thermal stratification and discrete high- and low-temperature regions of the TES system. A low-cost solid filler used to pack the single storage tank acts as the primary thermal storage medium and reduces the overall required quantities of the relatively higher cost molten salt heat transfer fluid, which is usually a "packed-bed" of aggregate and sand [1]. As thus the STTC provides a more cost-effective option for TES systems with a potential cost reduction of 20%–37% compared to the two-tank system [2].

Since the advantage of cost reduction, the STTC TES system is progressively becoming an important research topic. A small pilot-scale packed-bed molten salt thermocline system has been successfully demonstrated in Sandia National Laboratories [3]. M.M. Valmiki et al. [4] presents an experimental study of the energy charge and discharge processes in a small oil packed bed thermocline thermal storage tank.

Some research efforts have led to the development of nitrate salt mixtures with low melting temperatures and high thermal stabilities for CSP applications [5]. Solid materials for high temperature thermal energy storage system in CSP have also been widely investigated [6].

Yang and Garimella [7,8] carried out a series of numerical investigations on the molten-salt packed-bed thermocline system using the developed two-temperature model. Li et al. [9] presented dimensionless heat transfer governing equations for fluid and solid fillers for the packed-bed thermocline TES and studied various scenarios of thermal energy charging and discharging processes. Xu et al. [1,10,11] presented a transient two-dimensional dispersion-concentric model to investigate the discharging behavior of the packed-bed thermocline tank. A parametric analysis was carried out and various influencing factors were analyzed. Different one-dimensional models were also proposed [12–15]. Mario Biencinto [16] developed a simulation model for solar thermal power plants with a thermocline storage tank with logistic function in TRNSYS, and assessed different operation strategies.

Entropy generation and exergy transport were monitored to investigate the influence of internal granule diameter and external convection losses on tank performance [17]. External convection losses strongly influence entropy generation inside the tank fillerbed due to the development of radial temperature gradients and increased irreversible thermal diffusion. The analysis in Ref. [18] showed that, for packed beds, sensible heat storage systems can provide much higher exergy recovery as compared to phase change material storage systems under similar high temperature storage conditions.

2. General considerations and description of the study

Though a lot of research efforts have been focused on the STTC TES system, most of the above studies were focused on evaluating the thermal performance of cylindrical type tank without insert liner. In practical some of the critical design consideration and the inherent flaws associated with the STTC TES system need to be solved:1) the high temperature and corrosion of the molten salt, 2) the limited height of the tank, 3) the thermal ratcheting of tank's wall. These would cause different physical boundary conditions with former research.

The first problem can be solved by the complicated wall of the thermocline tank. The single-tank thermocline (STTC) tank used in CSP plants at an industrial scale usually has a "sandwich configuration" side wall construction consisting of multiple layers [7,19–21]: an inner firebrick layer for thermal isolation, a steel shell layer for mechanical support and an outer layer for corrosion protection and thermal insulation. To inhibit leakage and corrosion of molten salt through the internal insulation, an incoloy or AISI 321H stainless steel insert liner is installed between the rock packed bed and insulation, which is corrugated in both the horizontal and longitudinal directions to accommodate thermal expansion and

contraction associated with the operation of the thermocline [19,20].

Usually, the length scale of these corrugations is assumed to be smaller than the size of the granular filler, inhibiting full contact with the rock and preventing crushing of the liner. Due to the small relative thickness of the corrugated liner, its thermal effects are neglected. However, solid particles small enough should be utilized as solid fillers in the STTC system to achieve high system performance and efficiency [1]. Besides, small solid particles are preferred as low void fraction and less molten salt in the tank, thus less cost can be achieved. In this way, the thermal effect can not be neglected with small size filler.

It has been proved that narrower and taller tanks are preferred in designing a thermocline system with higher efficiency. Increasing the height of the tank improves the efficiency such that the volume of the tank can be reduced. And less salt is required to store a given amount of energy, which reduces the overall cost of the project. However, there are many design considerations that limit the height of the tank such as the maximum bearing capacity of the soil and earthquake code requirements. Due to the density of the salt and quartzite-sand mixture, it was determined that the maximum liquid level in the tank should be limited to 39 ft [2]. The second barrier can be solved by truncated cone shaped tank.

The third primary problem associated with STTC TES is the potential of thermal ratcheting of the tank's walls which occurs as repeated thermal cycles result in the settlement of the granular bed towards the base of the tank and the accumulation of the residual stresses. This can lead to catastrophic rupture of the tank's walls [22–27].

The hoop stress in the steel shell used for the prediction of thermal ratcheting was analyzed by Flueckiger et al. [22] through both a finite-element analysis and simple strain relations, they found that failure was prevented when the peak hoop stress is less than the material yield strength of the steel shell and the insulation between the steel shell and the filler region should be maximized in order to avoid ratcheting without incurring excessive energy loss. The elasto-plastic behavior of the quartzite material bed in a proposed commercial-scale power-tower thermocline system was investigated with the Drucker-Prager model in ANSYS by G.J. Kolb [23]. It showed that ratcheting failure could occur or not highly depends on the mechanical properties of quartzite gravel filler. Another study also investigated thermal ratcheting in the thermocline storage tank at the Solar One facility through a finite element model with the infinite rigidity approximation of internal granular, the results were compared with data from strain gauges on the tank [24]. The findings indicated that the hoop stress developed during typical operation is too low to rupture the tank with a relatively small operating temperature range considered: 204°C–304 °C. However, the increase in energy storage temperature ranges will lead to an accelerated and more severe level of thermal ratcheting.

One of the solutions that can avoid the issue of thermal ratcheting proposed by Brown et al. [25] is to replace the packed aggregate bed with structured concrete. However, the maximum reported system efficiency of the designed structured concrete thermocline (SCTC) with the operating temperatures up to 585 °C (65%) is quite low. Strasser proposed an improved concrete thermocline configuration incorporating rows of parallel concrete plates reporting an increased system efficiency of 84% is reported based upon numeric modeling results [26], which is still lower than the packed-bed thermocline (PBTC) efficiency (>93% [27]). Besides, based upon the modeling reported in ref. [28], it can be seen that the capacity cost of the PBTC is nearly 10% less than that of the SCTC, the LCOE of the plant with PBTC TES is nearly one-half of a cent less than that of the plant with SCTC TES. So in this way, the cost of decreasing the potential of thermal ratcheting is high.

The third barrier that of thermal ratcheting with rock solid media can also be addressed by using sloped walls and screens and meshes to create layers within the tank [29]. The advantage of the sloped-wall tank design is that thermal expansion may take place along the conical longitude [19].

A novel tank geometry with sloped tank wall is proposed in this study, which is a good solution to break the limit height of the tank determined by the maximum bearing capacity of soil and earthquake code requirements, and reduce the potential for the occurrence of thermal ratcheting with its truncated cone shaped tank and packed pebble bed assembly.

The rock particles packed in a large pile in the truncated cone shaped tank can be more stable than normal vertical tanks, and even allowed to form a self-supported packed bed by settling the rock particles undisturbed at the natural angle of repose. This prevents the particles slumping to fill the annular separation gap between the internal granular rock and tank wall created by the thermal expansion, especially with the help of layers created by screens and meshes within the tank. Thus, tank wall can return to its original dimensions and the build-up of residual mechanical stress in the tank shell through repeated operational cycles is prevented. And the tank has a truncated cone shape reducing the normal force on the walls during thermal expansion of the rocks by guiding them upwards [30,31].

To date, the influences of above critical design caused different physical boundary conditions on the thermal performance of STTC TES tank are still not well studied. In practical, the effect of insert liner should not be ignored if the relative size of liner to solid granular filler is not very small. So the thermal performance of thermocline tank with different sizes of insert liners are investigated for quantitative understanding of the effect of insert liner. At the same time, in order to take advantage of truncated cone shaped tank for the eradication of thermal ratcheting and increasing the maximum height of the tank, both while maintaining a good efficiency, thermal performance of different sizes of truncated cone shaped tanks are also needed to be investigated with the constraints of same tank volume and inlet mass flow rate.

To sum up, the objective of this work is to advance understanding of the effect of physical boundary condition on the molten-salt thermocline system. Quantitative understanding of this effect with the help of entropy generation analysis is essential to the evaluation of the influence of the insert liner and sloped tank wall on the fluid flow and the heat and mass transfer in packed beds, which is important to the successful design of thermocline packed bed system in CSP.

In this study, a transient two-dimensional and two-temperature model is developed to investigate the heat transfer and fluid dynamics in a molten salt thermocline thermal storage system. After model validation, the effects of physical boundary conditions on the thermal performance of thermocline storage system are investigated. The analysis of entropy generation distribution is done to replace the thermocline thickness and cut-off temperature discharging efficiency as the indicator for evaluating the performance of thermocline tank under different physical boundary conditions.

3. Mathematical model

3.1. Governing equations

The general layout of the thermocline storage system and the size of the inset liner are illustrated in Figs. 1 and 2 depicts the schematics of the truncated cone shaped molten salt thermocline tank. Excess hot HTF enters the top of the tank while cold HTF exits at the bottom to charge the thermocline. For subsequent discharge,

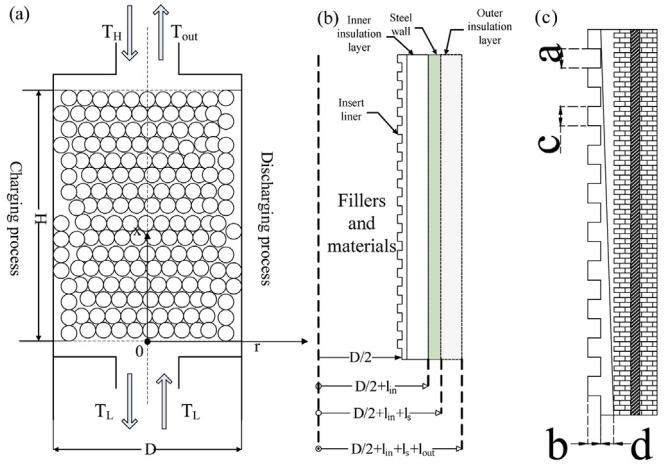

Fig. 1. Schematic diagram of the molten salt thermocline TES (a), the computational domain (b) and the size of the inset liner (c).

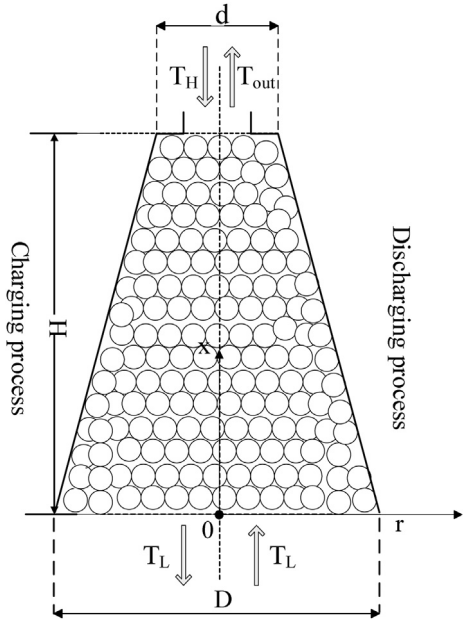

Fig. 2. Schematic diagram of the truncated cone shaped molten salt thermocline tank.

the flow is reversed so that cold HTF is pumped in at the bottom while hot HTF exits at the top.

The following assumptions are employed to simplify the analysis:

(1) The fluid flow and heat transfer are symmetrical about the axis.
(2) The distributors are not included in the computational domain and plug flow is imposed at the inlet of the filler region.
(3) The flow of molten salt is laminar and incompressible.
(4) The solid fillers are spherical particles with the same diameter and constant properties.

Continuity equation:

$$\frac{\partial \varepsilon \rho_l}{\partial t} + \nabla \cdot (\rho_l \vec{v}) = 0 \tag{1}$$

The momentum flux in the porous packed-bed is governed by Darcy's Law with the Brinkman–Forchheimer extension, Momentum equation:

$$\frac{\partial (\rho_l \vec{v})}{\partial t} + \nabla \cdot \left(\rho_l \frac{\vec{v}\vec{v}}{\varepsilon} \right) = -\varepsilon \nabla p + \nabla \cdot (\mu \nabla \vec{v}) + \varepsilon \rho_l \vec{g} + \varepsilon \left(\frac{\mu}{K} + \frac{F}{\sqrt{K}} \rho_l v_{mag} \right) \vec{v} \tag{2}$$

where $K = \frac{d_p^2 \varepsilon^3}{150(1-\varepsilon)^2}$, $F = \frac{1.75}{\sqrt{150\varepsilon^3}}$. In the axisymmetric coordinate system shown in Figs. 1 and 2, the problem is two-dimensional, incompressible fluid: $\nabla = \vec{e_r}\frac{\partial}{\partial r} + \frac{\vec{e_\theta}}{r}\frac{\partial}{\partial \theta} + \vec{e_x}\frac{\partial}{\partial x}$, $\vec{v} = v_r\vec{e_r} + v_x\vec{e_x}$.

As the volume expansion/shrinkage, viscous effects and kinetic energy changes the conduction or convection terms are omitted, Energy equation for the molten salt:

$$\frac{\partial \left(\varepsilon \rho_l C_{p,l} T_l \right)}{\partial t} + \nabla \cdot \left(\rho_l \vec{v} C_{p,l} T_l \right) = \nabla \cdot \left(k_{l,eff} \nabla T_l \right) + h(T_s - T_l) \tag{3}$$

where the effective thermal conductivity of fluid and fluid to solid interstitial heat transfer coefficient [10]:

$$k_{l,eff} = \varepsilon k_l, \quad h_v = \frac{6(1-\varepsilon) k_f \left(2 + 1.1 \mathrm{Re}_p^{0.8} \mathrm{Pr}^{1/3} \right)}{d_p^2}$$

Energy equation for the solid fillers:

$$\frac{\partial \left((1-\varepsilon) \rho_s C_{p,s} T_s \right)}{\partial t} = \nabla \cdot \left(k_{s,eff} \nabla T_s \right) - h_i (T_s - T_l) \tag{4}$$

where the effective thermal conductivity of solid [10]:

$$k_{s,eff} = k_s \left(\frac{3(1-\varepsilon)^2}{3.6 \times 10^{10}} \frac{59.8 d_p}{2} \right)^{1/3} \frac{1}{0.531 d_p} + k_f \left[1 - \sqrt{1-\varepsilon} + \frac{2\sqrt{1-\varepsilon}}{1-\kappa} \left[\frac{(1-\kappa)\beta}{(1-\kappa\beta)^2} \ln \left(\frac{1}{\kappa\beta} \right) - \frac{\beta+1}{2} - \frac{\beta-1}{1-\kappa\beta} \right] \right],$$

$$\kappa = \frac{k_l}{k_s}, \quad \beta = 1.25 \left(\frac{1-\varepsilon}{\varepsilon} \right)^{10/9}.$$

Energy equation for the insulation layers and tank steel wall:

$$\frac{\partial \left(\rho_i C_{p,i} T_i \right)}{\partial t} = \nabla \cdot (k_i \nabla T_i) \tag{5}$$

Convection processes through fluid-saturated porous media are inherently irreversible, due partly to the transfer of heat in the direction of finite temperature gradients and partly to the viscous flow through the pores. The entropy generation rate per unit volume of homogeneous porous medium in the packed-bed thermocline tank for liquid is a function of both thermal diffusion and viscous dissipation [17,32]:

$$\dot{S}_{gen,l}''' = \frac{k_{l,eff} (\nabla T_l)^2}{T_l^2} + \frac{\mu \Phi}{T_l} \tag{6}$$

As thermal diffusion between the solid granules is not neglected in equation (4), the entropy generation equation for solid in the thermocline tank can be derivated as:

$$\dot{S}'''_{gen,l} = \frac{k_{s,eff}(\nabla T_s)^2}{T_s^2} \tag{7}$$

where $(\nabla T)^2 = \left(\frac{\partial T}{\partial x}\right)^2 + \left(\frac{\partial T}{\partial y}\right)^2 + \left(\frac{\partial T}{\partial z}\right)^2$,

$$\Phi = 2\left\{\left(\frac{\partial u}{\partial x}\right)^2 + \left(\frac{\partial v}{\partial y}\right)^2 + \left(\frac{\partial w}{\partial z}\right)^2\right\} + \left(\frac{\partial u}{\partial y} + \frac{\partial v}{\partial x}\right)^2 + \left(\frac{\partial v}{\partial z} + \frac{\partial w}{\partial y}\right)^2 + \left(\frac{\partial w}{\partial x} + \frac{\partial u}{\partial z}\right)^2 - \frac{2}{3}\left(\frac{\partial u}{\partial x} + \frac{\partial v}{\partial y} + \frac{\partial w}{\partial z}\right)^2$$

The total entropy generation of the STTC tank in the charging or discharging process can be obtained by equation (8):

$$S_{total} = \iint\left(\dot{S}'''_{gen,l} + \dot{S}'''_{gen,s}\right)\mathrm{d}V\mathrm{d}t \tag{8}$$

Non-dimensional form of equations (1)–(4) can be presented as following:

$$\frac{1}{\mathrm{Re}}\frac{\partial \varepsilon \Phi_{\rho l}}{\partial \tau} + \tilde{\nabla}\cdot\left(\Phi_{\rho l}\vec{V}\right) = 0 \tag{9}$$

$$\frac{\partial\left(\Phi_{\rho l}\vec{V}\right)}{\partial\tau} + \mathrm{Re}\tilde{\nabla}\cdot\left(\Phi_{\rho l}\frac{\vec{V}\vec{V}}{\varepsilon}\right) = -\mathrm{Re}\varepsilon\tilde{\nabla}P + \tilde{\nabla}\cdot\bar{\bar{\pi}} + \varepsilon\Phi_{\rho l}Ri\mathrm{Re}\vec{e_x} + \varepsilon\left(\frac{\Phi_{\rho l}\Phi_{\nu l}}{Da} + \frac{F\mathrm{Re}}{\sqrt{Da}}\Phi_{\rho l}V_{mag}\right)\vec{V} \tag{10}$$

$$\mathrm{Pr}\frac{\partial\left(\varepsilon\Phi_{\rho l}\Phi_{Cpl}\Theta_l\right)}{\partial\tau} + \mathrm{PrRe}\tilde{\nabla}\cdot\left(\Phi_{\rho l}\vec{V}\Phi_{Cpl}\Theta_l\right) = \tilde{\nabla}\cdot\left(\Phi_{ke}\nabla\Theta_l\right) + \mathrm{Pr}Ec\left\{-P\tilde{\nabla}\cdot\vec{V} + tr\left[\tilde{\nabla}\left(\frac{\vec{V}}{\varepsilon}\right)\cdot\bar{\bar{\pi}}\right] + \frac{\vec{V}\cdot\vec{V}}{2\varepsilon}\times\frac{\partial\Phi_{\rho l}}{\partial\tau}\right\} + Nu_i(\Theta_s - \Theta_l) \tag{11}$$

$$\mathrm{Pr}\frac{\partial\left(\Omega_{\rho Cp}(1-\varepsilon)\Phi_{\rho s}\Phi_{Cps}\Theta_s\right)}{\partial\tau} = \Omega_k\tilde{\nabla}\cdot\left(\Phi_{ks}\tilde{\nabla}\Theta_s\right) - Nu_i(\Theta_s - \Theta_l) \tag{12}$$

where $X = \frac{x}{d_s}$, $\vec{V} = \frac{\vec{v}}{v_{in}}$, $\tau = \frac{tv_c}{d_s^2}$, $P = \frac{1}{\rho_c v_{in}^2}p$, $\tilde{\nabla} = d_s\nabla = \vec{e_r}\frac{\partial}{\partial R} + \frac{\vec{e_\theta}}{R}\frac{\partial}{\partial\theta} + \vec{e_x}\frac{\partial}{\partial X}$,

$$\Phi_\rho = \frac{\rho_l}{\rho_c},\quad \Phi_{\nu l} = \frac{\nu_l}{\nu_c},\quad \Phi_\mu = \frac{\mu_l}{\mu_c}\quad \Phi_{kl} = \frac{k_l}{k_c},\quad \Phi_{ke} = \frac{k_e}{k_c},$$
$$\Phi_{Cpl} = \frac{Cp_l}{Cp_c},\quad \Phi_{Cps} = 1,\quad \Phi_{\rho s} = 1,$$

$$\Omega_{\rho Cp} = \frac{\rho_s C_{p,s}}{\rho_{lc} C_{p,c}},\quad \Omega_k = \frac{k_s}{k_c},\quad \mathrm{Re} = \frac{d_s v_{in}}{\nu_l},\quad Da = \frac{K}{d_s^2},\quad Ri = \frac{d_s g}{v_{in}^2},$$

$$Nu = \frac{h_i d_s^2}{k_c},\quad \mathrm{Pr} = \frac{\nu_c\rho_c Cp_c}{k_c},\quad Ec = \frac{v_{in}^2}{Cp_c(T_h - T_c)},\quad \bar{\bar{\pi}} = \frac{d_s}{\rho_c\mu_c v_{in}}\bar{\bar{\tau}},\quad \Theta_l = \frac{T_l - T_c}{T_h - T_c},\quad \Theta_s = \frac{T_s - T_c}{T_h - T_c}.$$

Non-dimensional entropy generation rate per unit volume can be presented as following:

$$\mathrm{N}_s = \frac{d_s^2}{k_{eff}}\dot{S}'''_{gen} \tag{13}$$

3.2. Boundary conditions and initial conditions

Boundary conditions are summarized as following. At the beginning of the discharging process, it is assumed that the tank is filled with molten salt and solid fillers which have the same hot temperature, and the tank wall is in thermally equilibrium with the interior hot storage material and the outside ambient air with a velocity of 2 m/s.

BC1: bottom inlet; x = 0, 0 ≤ r < D/2; $v_x|_+ = v_{in}$, $v_r|_+ = 0$, $T_f\Big|_+ = T_{f,in}$, $\partial T_s/\partial x|_+ = 0$
BC2: top outlet; x = H, 0 ≤ r < D/2; $\partial v_x/\partial x|_- = 0$, $v_r|_- = 0$, $\partial T_f/\partial x\Big|_- = 0$, $\partial T_s/\partial x|_- = 0$

BC3: symmetry axis of the cylindrical tank; 0 ≤ x ≤ H, r = 0;

$$\partial v_x/\partial r|_+ = 0,\quad v_r|_+ = 0,\quad \partial T_f/\partial r\Big|_+ = 0,\quad \partial T_s/\partial r|_+ = 0$$

BC4: the inner surface of the insert liner or the sloped insulation inner layer;

$$v_x|_- = v_r|_- = 0,\quad k_{f,eff}\partial T_f/\partial x\Big|_- = k_{in}\partial T_{in}/\partial r|_+,\quad k_{s,eff}\partial T_s/\partial r\Big|_- = 0$$

BC5: two cross sections of the insulation layers and tank steel wall adjacency to the fluid inlet and outlet;
x = 0 or x = H, D/2 ≤ r ≤ D/2 + l_{in} + l_{out} + l_s; $\partial T_{in}/\partial x = \partial T_s/\partial x = \partial T_{out}/\partial x = 0$
BC6: outmost wall of the thermocline tank;
0 ≤ x ≤ H, r = D/2+l_{in} + l_{out} + l_s; $-k_{out}\partial T/\partial r|_+ = h(T_{out} - T_\infty)$,$Nu = hH/k = 0.664\mathrm{Re}_D^{0.5}\mathrm{Pr}^{0.5}$,-
$\mathrm{Re}_D = v_{air}D/\nu_{air}$where v_{air} and ν_{air} are the velocity and viscosity of ambient air, respectively.

3.3. Material properties

One kind of molten salt called Hitec, which is a ternary salt mixture of 53 wt% KNO_3/7 wt% $NaNO_3$/40 wt% $NaNO_2$, has been considered to replace the Solar Salt because of its low freezing point of 142 °C, and has been used as heat transfer fluid (HTF) in the STTC TES systems. Quartzite rocks and sands were suitable to be used as the low-cost solid fillers which provided the bulk of thermal capacitance of the thermal storage. Its compatibility and durability within molten salt has been validated.

A heat- and corrosion-resistant alloy (Incoloy 800 alloy) liner with waffle design is used as insert liner to prevent leakage and corrosion of the high temperature molten salt. Firebrick is used as the inner insulation layer. The external surface of the tank is protected by a coat of ceramic fiber insulation.

The thermo-physical properties of molten salt changing with temperature and other solid materials are listed in Table 1.

3.4. Numerical method

The computational domain is discretized into finite volumes. All the variables are stored at the centers of the mesh cells. A second-order upwind scheme is used for the convective fluxes, while a

Table 1
Physical properties of molten salt and solid materials.

Name	Molten salt Hitec [12]	Quartzite rock	Inconel 800 inert linner	Firebrick	Steel	Ceramic
Density (kg/m^3)	$\rho_l = 2084-0.732 \times T_l(^\circ C)$	2500	7940	2000	7800	1000
Specific heat capacity (J/kg K)	$C_{pl} = 1561.7$	830	460	1000	470	1000
Thermal conductivity (W/m K)	$k_l = 0.421-6.53 \times 10^{-4}(T_l-260)$	5.69	11.5	1	35	0.1
Viscosity (kg/ms)	$\mu_l = \exp[-4.343-2.0143 \times (\ln T_l-5.011)]$					

central-differencing scheme is used for discretizing the diffusion fluxes. Iterations at each time step are terminated when the dimensionless residuals for all equations drop below 10^{-4}. The computations are performed using the commercial software FLUENT through the SIMPLEC algorithm. User-defined functions are developed to account for Eqs. (2)–(4), (6), (7). Grid and time-step dependence are checked by inspecting results from different grid densities and time intervals. Based on this, $\Delta x = \Delta r = 0.01$ m and $\Delta t = 0.5$s are chosen as this setting results in a temperature along the line $r = 0$ throughout the discharge process that is within 5% of that for the case with $\Delta x = \Delta r = 0.005$ m and $\Delta t = 0.1$s.

4. Results and discussion

4.1. Model validation

The experimental results of Pacheco et al. [3], Valmiki M.M. et al. [4] and simulation results from an algebraic model [34,35] are used here to validate the numerical model.

In Ref. [3] an experimental 2.3-MWht thermocline tank was constructed with quartzite rock (0.1905 cm) along with silica sand (0.6 mm) to reduce the void fraction. The mass ratio of quartzite to sand was 2:1 and the final void fraction was 0.22. The tank was 5.9 m in height and 3.0 m in diameter, The working temperature range of molten salt was 290°C–390 °C with mass flow rate of 7.94 kg/s.

In Ref. [4] the thermocline tank is 0.241 m in diameter and the active thermal storage section in the thermocline tank is 0.767 m in height with mesh filters and metal frames at the top and bottom to ensure the tight packing of the filler material. The porosity of the packed bed in the thermocline tank was found to be 0.326 and the mass ratio of river pebbles (2 cm) to pea pebbles (0.5 cm) was 1.49:1. The volume flow rate of Xceltherm 600 VR synthetic oil was 1.25 L per minute with temperature range of 32.1 °C–126.8 °C.

As the thermocouples were buried in thermocline rock bed in the experiments [3,4], some of them were in contact with the rock while others may had been located exactly in the pore centers, both of the axial temperature profiles of the HTF and solid in the thermocline tank are presented for validation.

Except for the temperature profile of initial condition in Ref. [3] (Fig. 3a) showing some scatter, the numerical predictions from the simulations seem to be in good agreement with the experimental data from the literature in Fig. 3 within the experimental uncertainty.

4.2. The effect of insert liner

In order to investigate the effect of insert liner, the charging and discharging process in a thermocline tank with different sizes of liners are simulated. In the 9 different sizes of liners listed in Table 2, case 1–5 are used to investigate the effect of axial size of the liner–'a' and 'c', while case 5–9 are for the radial size of the liner–'b' and 'd'. Different groups in the 9 cases are summarized: (1) Case 1, 2 and 5 have the same size of 'a' and 'c', increasing from 1 cm to 4 cm (2) Case 3, 4 and 5 have the same size of the sum of 'a' and 'c', which is 4 cm. The ratio of 'a' and 'c' differs. (3) Case 5, 6 and 7 have the same size of 'b' and 'd', increasing from 1 cm to 4 cm (4) Case 5, 8 and 9 have the same size of the sum of 'b' and 'd', which is 4 cm. The ratio of 'b' and 'd' differs. Other parameters and properties used in the model: H = 5 m, D = 2 m, $l_{in} = l_{out} = 0.1$ m, $l_{st} = 0.02$ m, $\dot{m} = 2.51$ kg/s, $\varepsilon = 0.22$, d = 0.01905 m. The non-dimensional number range of the CFD model is: Pe = 4650.6–4753.5, Pr = 6.35–13.41, Re = 4.33–14.58, Bi = 196810–237300. The non-dimensional number in the case without liner by algebraic model (Figs. 4, 7 and 10) is: Pe = 4702.3, Pr = 7.96, Re = 8.86, Bi = 226983.

Fig. 4 shows the variation of thermocline thickness in the near-wall area and in the center during the discharging process. Thermocline thickness is defined as the covering length of the thermocline region and can be expressed as: $min\{H(T_{out}),H(T_{crit,h})\} - H(T_{crit,c})$ in discharging cycle and $H(T_{crit,h}) - max\{H(T_{out}),H(T_{crit,c})\}$ in charging cycle, where $T_{crit,h} = T_h - 5$ and

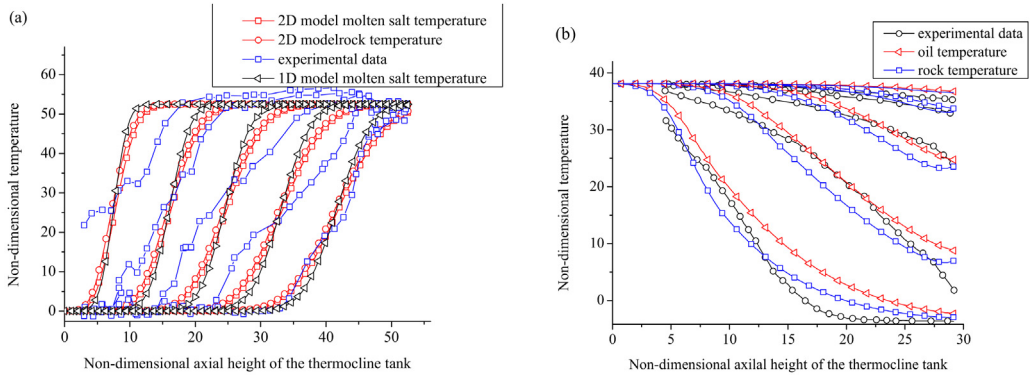

Fig. 3. (a). comparison between thermocline profiles from numerical results of 2-D model, 1-D algebraic model (Pe = 5586.800, Pr = 10.597, Re = 5.850, Bi = 328660.228) [34] and experimental results from Ref. [3] in a discharging cycle of the molten salt tank at time intervals of 30 min; (b) comparison between the numerical and experimental charging temperature distribution along the oil tank height at time intervals of 16 min from Ref. [4].

Table 2
Different insert liner cases and discharging efficiencies.

Case	a(cm)	b(cm)	c(cm)	d(cm)	$a + c/H$	$b + d/D$	a/a+c	b/b + d	Final discharging efficiency	Second-law discharging efficiency
1(a1c1)	1	2	1	2	0.004	0.04	0.5	0.5	94.05%	89.69%
2(a4c4)	4	2	4	2	0.016	0.04	0.5	0.5	95.09%	90.42%
3(a1c3)	1	2	3	2	0.008	0.04	0.25	0.5	93.35%	88.87%
4(a3c1)	3	2	1	2	0.008	0.04	0.75	0.5	95.16%	90.43%
5(a2c2)	2	2	2	2	0.008	0.04	0.5	0.5	94.13%	89.92%
6(b1d1)	2	1	2	1	0.008	0.02	0.5	0.5	95.56%	91.80%
7(b4d4)	2	4	2	4	0.008	0.08	0.5	0.5	93.24%	89.47%
8(b1d3)	2	1	2	3	0.008	0.04	0.5	0.25	94.65%	89.94%
9(b3d1)	2	3	2	1	0.008	0.04	0.5	0.75	93.64%	91.66%

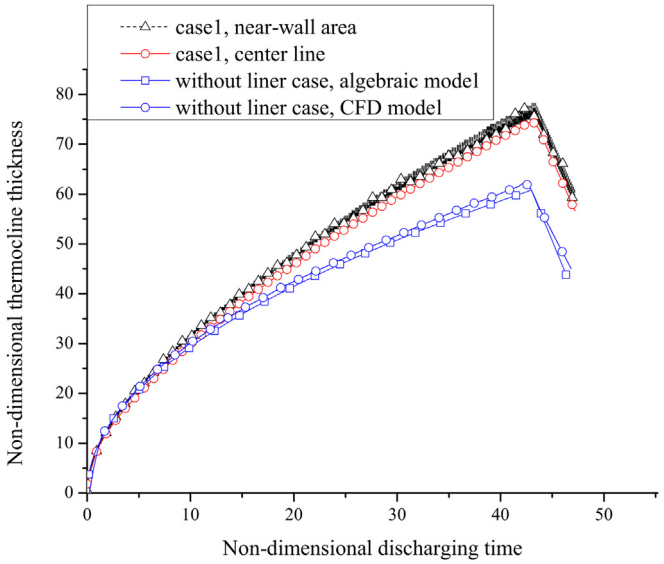

Fig. 4. Profiles of near-wall area and centerline thermocline thickness versus discharging time along the tank height for case. 1 and the profiles of thermocline thickness in the case without liner by CFD model and algebraic model from Ref. [34].

$T_{crit,c} = T_c + 5$ represent the critical low and hot temperatures for evaluating the thermocline thickness, respectively. Thermocline thickness is usually an important indicator for the thermal performance of the packed-bed thermocline storage tank.

In Fig. 4, the thermocline thickness increases sharply at the beginning, and then the increase becomes slower with the mixing in the thermocline region. The thickness climbs to a maximum value when the thermocline region arrives at the outlet, i.e., 1.4 m at 1.5 h, and then it decreases nearly linearly with the discharging of the thermocline region. Besides, Fig. 4 shows that the thermocline thickness is larger and much more fluctuate in the near-wall area along the tank height than that in the center of the tank, which means the thickness in the center is not accurate to evaluate the mixing and thermal performance of the thermocline tank, especially with the effect of insert liner boundary condition. The difference of thermocline thickness between without liner case and case 1, center line is caused by the disturbance of liner in fluid and the higher heat conductance of liner compared with the rock particles. For the without liner case, the thermocline thickness of CFD model is a little larger than that of the algebraic model in the whole discharging process, it is because the CFD model takes into account of the heat loss from the wall and the velocity distribution.

The discharging efficiency in Fig. 5 is defined as $\eta = \frac{\int_0^{t_{dc}} \dot{m} C_p (T_{out} - T_c) \mathrm{d}t}{Q_{store}}$. In Refs. [7,8,17], the authors enforced a temperature cut-off criterion to the outflow molten-salt discharge to account for the loss of thermal quality over time: $T_{out} > T_c + 0.95(T_h - T_c)$, so only salt outflow at temperatures above 95% of the total operating range was designated as being useful for power production. While in this work the hot molten-salt temperature necessary for this minimum output is 473 °C; thus any molten salt below this temperature is not utilizable for power production and will not be discharged from the thermocline tank [33]. So $T_{out} > 746.15$ K is considered useful in calculating the discharging efficiency.

The second-law efficiency of the thermocline tank in discharging process is defined as:

$$\eta_{II,dc} = \frac{\mathrm{Ex}_{out} - \mathrm{Ex}_{\mathrm{in}}}{\mathrm{Ex}_{TES}} \tag{14}$$

where $\mathrm{Ex}_{out} - \mathrm{Ex}_{\mathrm{in}} = \int_0^{t_{dc}} \dot{m} C p_{p,l} \left[\left(T_{out} - T_{in} \right) - T_0 C p_{p,l} \ln \frac{T_{out}}{T_{in}} \right] \mathrm{d}t.$

The exergy stored in the thermocline tank before the discharging process can be quantified according to Eq. (10),

$$\mathrm{Ex}_{TES} = \iiint_V \left\{ \left(\varepsilon \rho_l C p_{p,l} + (1-\varepsilon) \rho_s C p_{p,s} \right) \left[(T_h - T_c) - T_0 \ln \left(\frac{T_h}{T_c} \right) \right] \times \right\} \mathrm{d}V \tag{15}$$

Fig. 5 shows that the outlet temperature decreases fast after the thermocline region arriving at the outlet, and the discharging efficiency and second-law discharging efficiency become non-linear with discharging time. The final discharging efficiency for case 1 is 94.05%, while the final second-law discharging efficiency is 89.69%. The efficiencies of other cases are listed in Table 2. It is also found that the variation of second-law discharging efficiency with insert liner sizes is the same with discharging efficiency.

In Fig. 6 it is found that the radial temperature difference of centerline and near-wall axial line is largest in case 1(Fig. 6a) and case3 (Fig. 6b). The reason is that the smaller value in Ref. $a + c/H$ of case 1 and a smaller value of $a/a + c$ resulting in larger average velocity in case 3. The fluctuations in near-wall axial temperature distribution of case 2, 4 and 5 are caused by the smaller characteristic size of insert layer (a and c) compared with the diameter of solid particles.

Fig. 7 shows the case 4 has the smallest and slowest thermocline thickness, and thermocline thickness in case2 is very close to case 4, implying that the disturbance in temperature gradient caused by corrugated liner is the smallest. The thermocline thickness for case 5 is in the middle, then following with case1 and case 3.

As the thermocline thickness in the center of the tank and the discharging efficiency does not clearly and accurately reflect the variation of the effect of different insert liners, entropy generation analysis have been done for comparison and finding patterns.

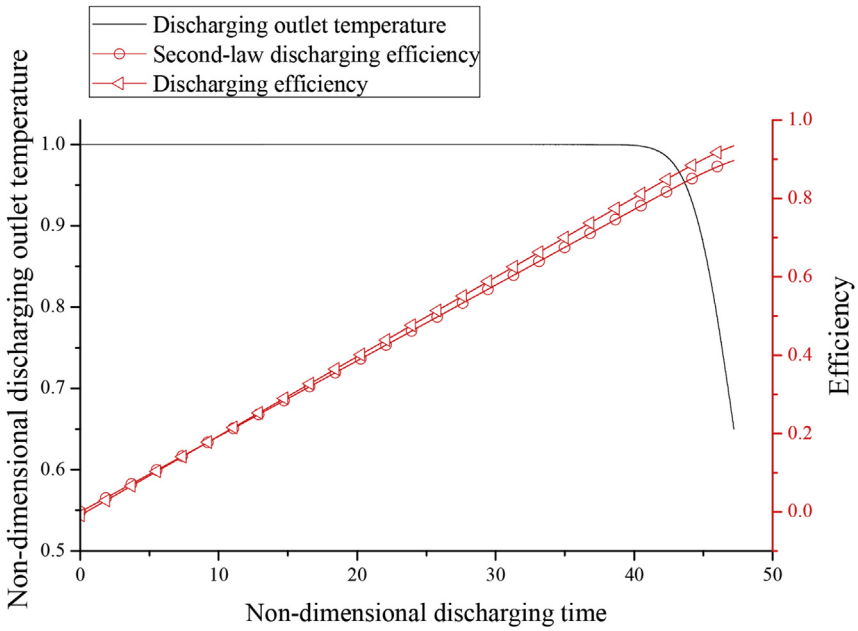

Fig. 5. Profiles of outlet temperature and discharging efficiency in the discharging process for case. 1.

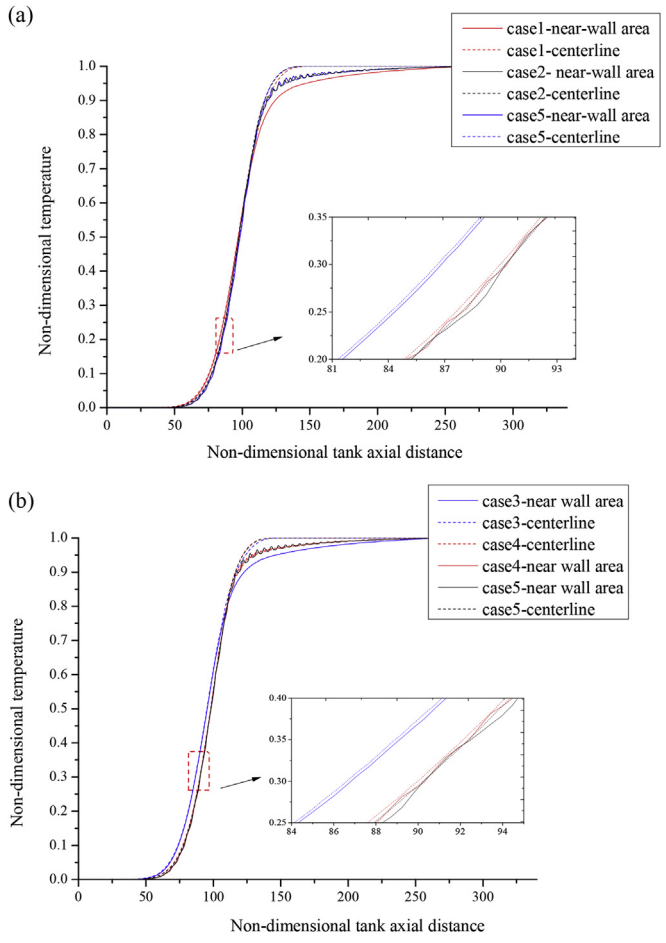

Fig. 6. Variations in the near-wall (0.01 m form the insert liner) axial line and centerline molten salt temperature profiles of case 1–3 (a); case3–5 (b) for insert liner in the charging process at 7200s.

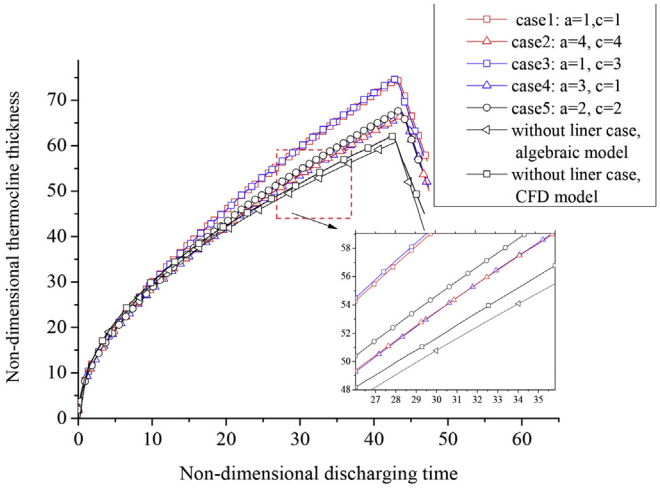

Fig. 7. Variations in the thermocline thickness profiles of case 1–5 and the case without liner by CFD model and algebraic model from Ref. [34] in the discharging process.

Though the entropy generation rate per unit volume of homogeneous porous medium in the packed-bed thermocline tank for liquid is a function of both thermal diffusion and viscous dissipation, viscous dissipation is omitted from the entropy generation analysis as it is too small compared with thermal diffusion effect [17].

Molten salt and solid control volume entropy generation rate distribution are investigated in Fig. 8. It shows that solid and molten salt entropy generation are mainly distributed in the thermocline region and solid entropy generation rate is much larger than molten salt entropy generation rate because its larger thermal conductivity.

The final total entropy generation of the thermocline heat storage system can also be calculated as following:

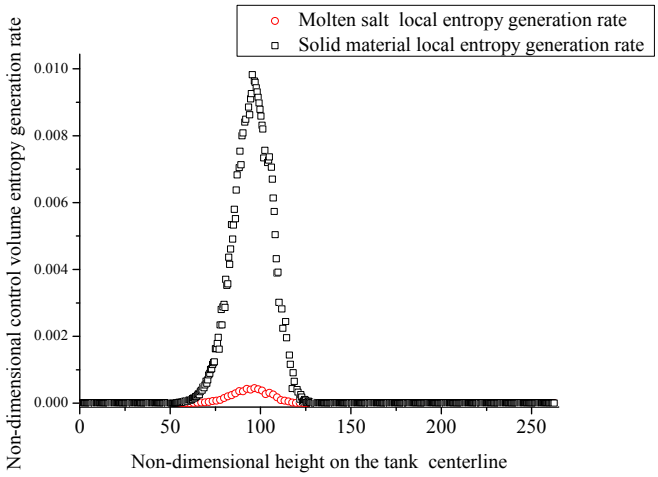

Fig. 8. Molten salt and solid control volume entropy generation rate distribution for case 6 at 7200s in the discharging process.

$$S_g = \Delta S - S_{flow} = \iiint_V \left\{ \varepsilon \rho_l Cp_{p,l} \ln\left(\frac{T_l}{T_h}\right) + (1-\varepsilon)\rho_s Cp_{p,s} \ln\left(\frac{T_s}{T_h}\right) \right\} dV - \int_0^{t_{dc}} \dot{m} Cp_{p,l} \ln\frac{T_{in}}{T_{out}} dt \quad (16)$$

It is used to validate the simulated total entropy generation from equation (8). The two approaches are found to yield almost identical results. The errors of total entropy generation results between two different methods are acceptable (less than 10%).

Fig. 9 shows that the variation of entropy generation with liner sizes in the discharging time is different between molten salt entropy generation and solid generation. That is caused by the difference in molten salt and solid temperature gradient, especially in the area close to the insert liner. The variation of molten salt entropy generation with liner sizes is the same with thermocline thickness. The variation of total entropy generation with liner sizes is the same with solid entropy generation as the solid entropy generation is larger. Case 4 has the smallest and slowest total entropy generation, following by case 2, 5, 3, and 1.

The reason of this variation is that case 4 has the largest concave area and thus the smallest average velocity. It is known that lower velocity of the molten salt in the thermocline tank leads to smaller thermocline thickness. While for case 2, the reason is that it has less small convexes and concaves, resulting in less disturbance to the flow though the average velocity is not that small as that in case 4. It can be concluded that the axial convex size of liner should be as small as possible.

The radial size of insert liner has also been investigated by comparing with the thermocline thickness and entropy generation of different sizes.

In Fig. 11, case 6 has the smallest and slowest total entropy generation, following with case 9, 5, 7 and 8, which is a little different with the variation of thermocline thickness and molten salt entropy generation in different cases.

The variation of total entropy generation is regarded as more accurate with all of the fluid domain taken into consideration. The reason of the variation is that smaller radial size causes less disturbance and smaller average velocity in the flow domain. It can

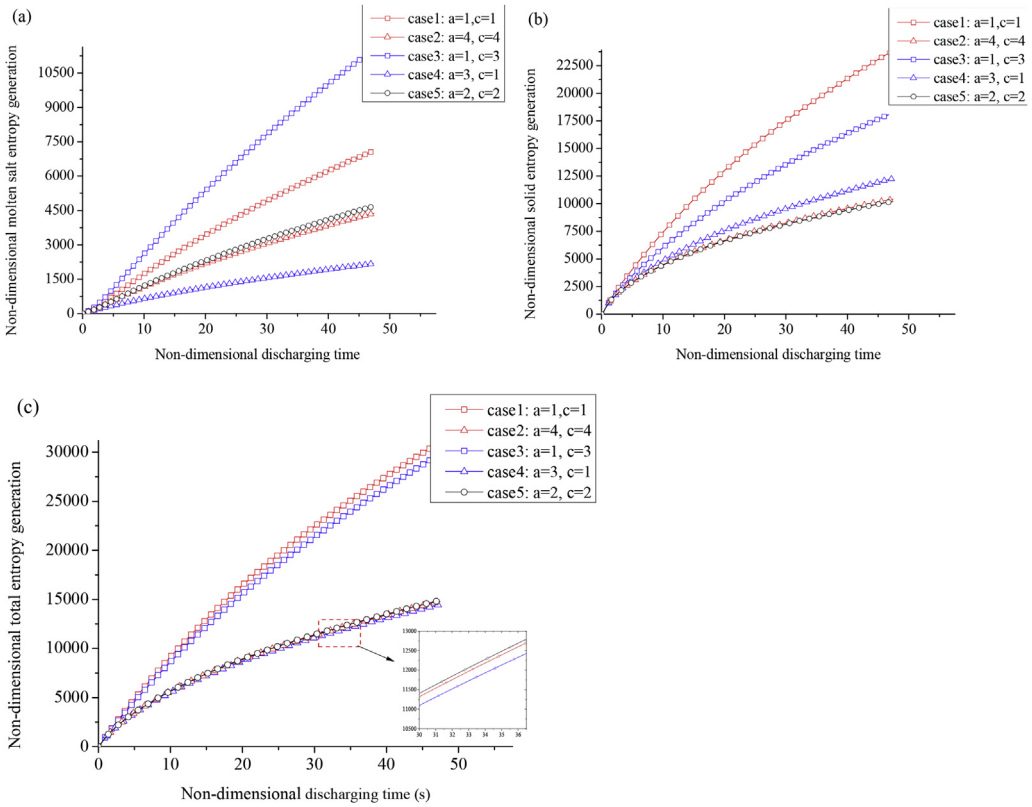

Fig. 9. Variations in the entropy generation in the thermocline tank of case 1–5 in the discharging process: (a) molten salt entropy generation; (b) solid entropy generation; (c) total entropy generation.

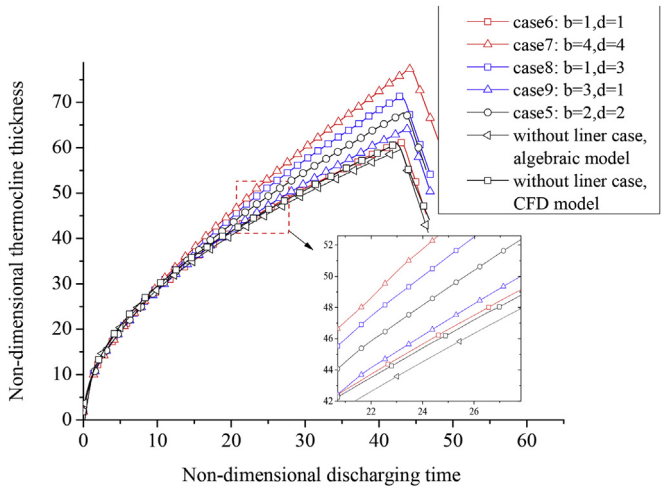

Fig. 10. Variations in the thermocline thickness profiles of case 5–9 and the case without liner by CFD model and algebraic model from Ref. [34] in the discharging process.

be concluded that the radial size of the insert liner should also be as small as possible.

4.3. The effect of sloped tank wall

A novel tank geometry with sloped tank wall is proposed in this study, which is a good solution to break the limit height of the tank determined by the maximum bearing capacity of soil, and reduce the potential for the occurrence of thermal ratcheting with its truncated cone shaped tank and packed pebble bed assembly. In order to take advantage of truncated cone shaped tank for the eradication of thermal ratcheting and increasing the maximum height of the tank, both while maintaining a good efficiency, thermal performance including thermocline thickness and entropy generation of different sizes of truncated cone shaped tanks are investigated with the constraints of same working temperature range 290 °C −560 °C, same tank volume of 15.7 m^3 and same inlet mass flow rate of 2.51 kg/s. The simulations are completed in the whole charging-discharging cycle including a charging half cycle and sequent discharging half cycle both with the cut-off temperature of 473 °C for comprehensive understanding of the effect of the sloped tank wall.

Table 3
Different sizes of sloped wall tanks and a regular cylindric tank.

Case	d(m)	D(m)	H(m)	V_{tank} (m^3)	Inclined angle (degree)
1	1.57	2.40	5.00	15.70	85.26
2	1.93	2.20	5.00	15.70	88.45
3	1.33	2.60	5.00	15.70	82.76
4	1.57	2.84	4.00	15.70	80.98
5	1.57	2.07	6.00	15.70	87.61
6	2.07	2.40	4.00	15.70	87.63
7	1.18	2.40	6.00	15.70	84.20
8	2.00	2.00	5.00	15.70	90.00

The 7 different sizes of sloped wall tanks and a regular cylindrical tank are listed in Table 3. Different groups in the 7 cases are summarized: (1) case 1, 2 and 3 have different top areas and bottom areas; (2) case 1, 4 and 5 have different bottom areas and tank heights in the truncated cone shaped tank; (3) case 1, 6 and 7 have different top areas and tank heights; Besides, case 8 is a regular cylindrical tank for comparison which has the same tank height and tank volume with case 1.where the inclined angle is defined as $arctan(2H/D - d)$.

The Variations in the thermocline thickness profiles in Fig. 12

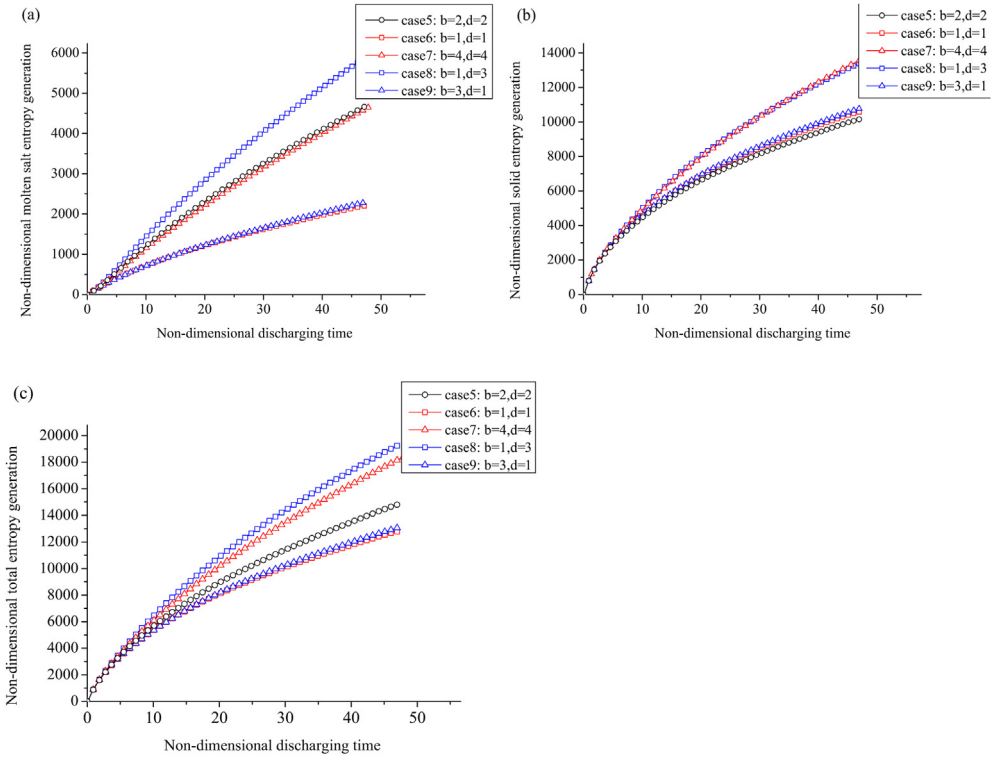

Fig. 11. Variations in the entropy generation in the thermocline tank of case 5–9 in the discharging process: (a) molten salt entropy generation; (b) solid entropy generation; (c) total entropy generation.

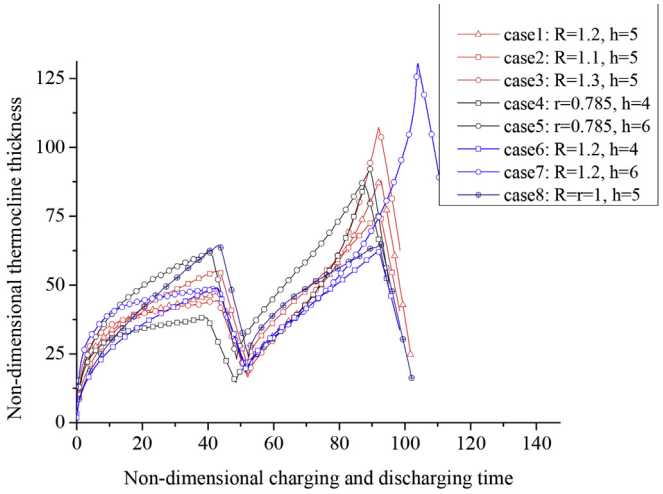

Fig. 12. Variations in the thermocline thickness profiles of case 1–8 in the discharging process.

show that:

(1) Most of the truncated cone shaped tank cases have larger thermocline thickness than the regular cylindrical tank with same tank volume except case 6, which is caused by the large inclined angle of the sloped wall and small tank height.
(2) The truncated cone tank of case 2 has the smallest peak value of thermocline thickness in the charging half cycle compared with case 1 and 3, while the largest thermocline thickness peak value in the discharging half cycle. The truncated cone tank of case 2 has less charging time compared with regular cylindrical tank at the same tank height and tank volume.
(3) In the group of case 1, 4 and 5; case 5 has the largest and fastest thermocline thickness compared with case 1 and 4. It is the same that case 7 has the largest and fastest thermocline thickness compared with case 1 and 6 in the charging-discharging cycle. It shows that larger height of thermocline tank causes larger thermocline thickness with the same tank volume.

The thermocline thickness in case 7 is also larger than that in case 5, it indicates that larger inclined angle of the sloped wall causes smaller thermocline thickness with the same tank height and tank volume.

As the case 1, 4 and 5 have same top area, the charging cut-off time and themocline thickness at charging cut-off time is very close. The close discharging cut-off time and themocline thickness at discharging cut-off time in case 1, 6 and 7 is caused by the same bottom area.

The variations in the entropy generation in Fig. 13 show that:

(1) The variations of molten salt entropy generation and solid entropy generation in the truncated cone thermocline tank cases are the same.
(2) Most of the truncated cone shaped tank cases have larger and faster entropy generation than the regular cylindrical tank with same tank volume except case 5 and case 2, which is caused by the largest tank height in case 5 and the largest inclined angle of the sloped wall in case 2.
(3) The truncated cone thermocline tank of case 2 tank has the largest entropy generation in the charging half cycle compared with case 1 and 3, while the smallest entropy generation in the discharging half cycle. It is found that larger inclined angle of the sloped wall causes smaller thermocline thickness and entropy generation with the same tank height and tank volume, and there is a positive correlation between the thermocline thickness and entropy generation with the same tank height and volume.

It also shows that truncated cone shaped tank has advantage in the charging process with low entropy generation in molten salt and solid material, while it goes against the discharging process. On the whole the truncated cone shaped tanks have worse thermal performance compared regular cylindric tank at the same tank height and tank volume.

(4) In the group of case 1, 4 and 5, case 5 has the largest and fastest thermocline thickness yet the smallest entropy generation compared with case 1 and 4. It is the same that case 7 has the largest and fastest thermocline thickness yet smallest entropy generation compared with case 1 and 6 in the charging and discharging cycle. It is found that larger tank height causes larger thermocline thickness and smaller entropy generation in the truncated cone shaped tanks with the same tank volume.

The thermocline thickness and entropy generation in case 7 are also larger than those in case 5, it indicates that larger inclined angle of the sloped wall causes smaller thermocline thickness and entropy generation with the same tank height and tank volume.

5. Conclusion

In this study, a transient two-dimensional and two-temperature model is used to investigate the heat transfer and fluid dynamics in a molten salt thermocline thermal storage system. After model validation, the effects of physical boundary conditions including insert liner and sloped wall on the thermal performance of thermocline storage system are investigated with the method of entropy generation analysis.

(1) The thermocline thickness is larger and much more fluctuate in the near-wall area along the tank height than that in the center of the tank under the insert liner boundary condition, which means the thickness in the center is not accurate to evaluate the mixing and thermal performance of the thermocline tank.
(2) Smaller value in $a + c/H$ and larger average velocity cause larger radial temperature difference. The larger characteristic size of insert liner compared with the diameter of solid particles causes fluctuations in near-wall axial temperature distribution. It is found that both of the axial and radial convex size of liner should be as small as possible, resulting in smaller average velocity and less disturbance in the flow.
(3) Solid and molten salt entropy generation are mainly distributed in the thermocline region and solid entropy generation rate is much larger than molten salt entropy generation rate because its larger thermal conductivity.
(4) The truncated cone shaped tank has advantage in the charging process with low entropy generation in molten salt and solid material, while it goes against the discharging process. On the whole the truncated cone shaped tanks have worse thermal performance compared regular cylindrical tank at the at same tank height and tank volume.

It is found that larger inclined angle of the sloped wall causes smaller thermocline thickness and entropy generation with the same tank height and tank volume for truncated cone shaped tanks.

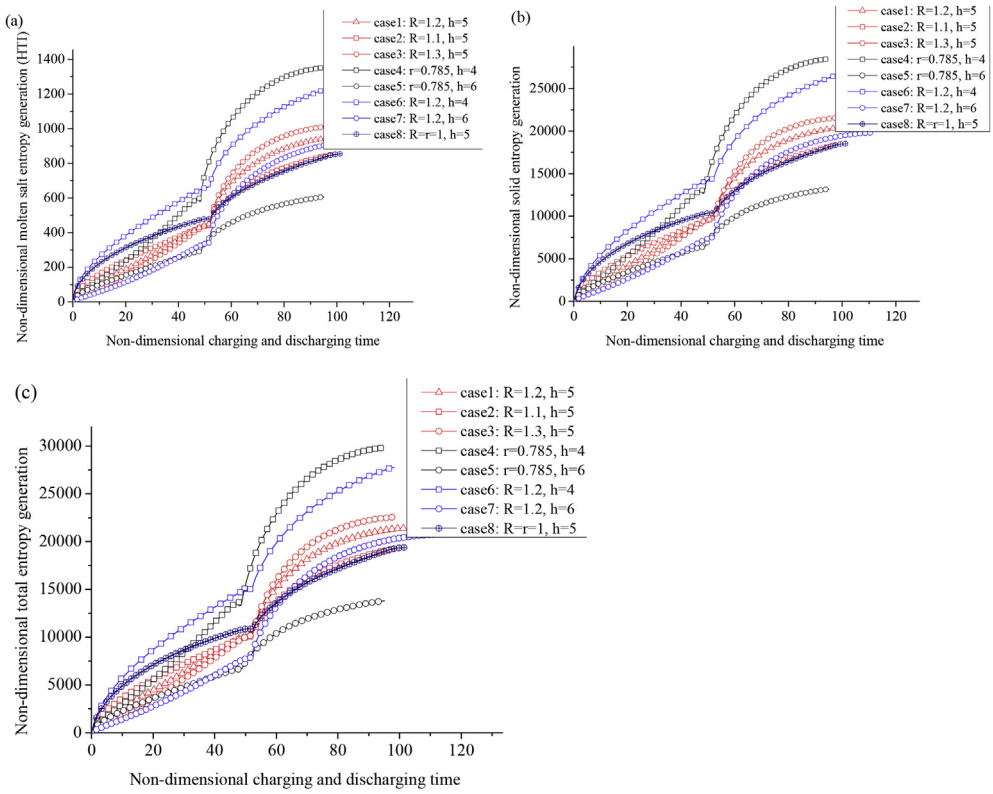

Fig. 13. Variations in the entropy generation in the truncated cone thermocline tank of case 1–8 in the discharging process: (a) molten salt entropy generation; (b) solid entropy generation; (c) total entropy generation.

(5) Larger tank height causes larger thermocline thickness and smaller entropy generation in the truncated cone shaped tanks with the same tank volume.

Acknowledgements

This work is supported by the Beijing Municipal Science & Technology Commission (D121100001012001), China National Hi-Tech R&D (863 Plan) (2013AA050502), Beijing Natural Science Foundation (3164052), Guangdong Innovative and Entrepreneurial Research Team Program (No. 2013N070), and the National Natural Science Foundation of China (No. 51476164).

References

[1] C. Xu, X. Li, Z.F. Wang, et al., Effects of solid particle properties on the thermal performance of a packed-bed molten-salt thermocline thermal storage system, Appl. Therm. Eng. 57 (2013) 69–80.
[2] Electric Power Research Institute, Solar Thermocline Storage Systems: Preliminary Design Study, 2010, p. 1019581. Palo Alto, CA.
[3] J.E. Pacheco, S.K. Showalter, W.J. Kolb, Development of a molten-salt thermocline thermal storage system for parabolic trough plants, J. Sol. Energy Eng. 124 (2002) 153–159.
[4] M.M. Valmiki, W. Karaki, P. Li, et al., Experimental investigation of thermal storage processes in a thermocline tank, J. Sol. Energy Eng. 134 (4) (2012) 041003.
[5] T. Bauer, D. Laing, R. Tamme, Recent Progress in Alkali Nitrate/Nitrite Developments for Solar Thermal Power Applications, Molten Salts Chemistry and Technology, MS9, Trondheim, Norway, 2011.
[6] X. Py, N. Calvet, R. Olives, P. Echegut, C. Bessada, F. Jay, Thermal storage for solar power plants based on low cost recycled material, in: The 11th International Conference on Thermal Energy Storage Effstock, 2009. Stockholm, Sweden.
[7] Z. Yang, S.V. Garimella, Molten-salt thermal energy storage in thermoclines under different environmental boundary conditions, Appl. Energy 87 (2010) 3322–3329.
[8] Z. Yang, S.V. Garimella, Cyclic operation of molten-salt thermal energy storage in thermoclines for solar power plants, Appl. Energy 103 (2013) 256–265.
[9] P. Li, J.V. Lew, W. Karaki, et al., Generalized charts of energy storage effectiveness for thermocline heat storage tank design and calibration, Sol. Energy 85 (2011) 2130–2143.
[10] C. Xu, Z.F. Wang, Y.L. He, et al., Sensitivity analysis of the numerical study on the thermal performance of a packed-bed molten salt thermocline thermal storage system, Appl. Energy 92 (2012) 65–75.
[11] C. Xu, Z.F. Wang, Y.L. He, et al., Parametric study and standby behavior of a packed-bed molten salt thermocline thermal storage system, Renew. Energy 48 (2012) 1–9.
[12] P. Li, J.V. Lew, W. Karaki, et al., Generalized charts of energy storage effectiveness for thermocline heat storage tank design and calibration, Sol. Energy 85 (2011) 2130–2143.
[13] A. Modi, C.D. Pérez-Segarra, Thermocline thermal storage systems for concentrated solar power plants: one-dimensional numerical model and comparative analysis, Sol. Energy 100 (2014) 84–93.
[14] Z. Yang, S.V. Garimella, Thermal analysis of solar thermal energy storage in a molten-salt thermocline, Sol. Energy 84 (2010) 974–985.
[15] R. Bayon, E. Rojas, Simulation of thermocline storage for solar thermal power plants: from dimensionless results to prototypes and real size tanks, Int. J. Heat Mass Transf. 60 (2013) 713–721.
[16] M. Biencinto, R. Bayon, E. Rojas, et al., Simulation and assessment of operation strategies for solar thermal power plants with a thermocline storage tank, Sol. Energy 103 (2014) 456–472.
[17] S.M. Flueckiger, S.V. Garimella, Second-law analysis of molten-salt thermal energy storage in thermoclines, Sol. Energy 86 (2012) 1621–1631.
[18] H. Bindra, P. Bueno, J.F. Morris, et al., Thermal analysis and exergy evaluation of packed bed thermal storage systems, Appl. Therm. Eng. 52 (2013) 255–263.
[19] K.Y. Wang, R.E. West, F. Kreith, et al., High-temperature sensible-heat storage options, Energy 10 (10) (1985) 1165–1175.
[20] G.J. Kolb, U. Nikolai, Performance Evaluation of Molten Salt Thermal Storage Systems, Sandia National Laboratories, 1988. SAND87–3002.
[21] R. Gabbrielli, C. Zamparelli, Optimal design of a molten salt thermal storage tank for parabolic trough solar power plants, J. Sol. Energy Eng. 131 (2009) 041001–041010.
[22] S. Flueckiger, Z. Yang, S.V. Garimella, An integrated thermal and mechanical investigation of molten-salt thermocline energy storage, Appl. Energy 88 (2011) 2098–2105.
[23] G. J. Kolb, G. Lee, P. Mijatovic, et al., Thermal ratcheting Analysis of Advanced Thermocline Energy Storage Tanks, SAND2011-5312C 463880, Sandia National Laboratories, Albuquerque, NM.
[24] S.M. Flueckiger, Z. Yang, S.V. Garimella, Thermomechanical simulation of the

solar one thermocline storage tank, J. Sol. Energy Eng. 134 (041014) (2012) 1–6.
[25] B. Brown, M. Strasser, R.P. Selvam, Development of a Structured Thermocline Thermal Energy Storage System, Proc. ASES-0074, 2012.
[26] M.N. Strasser, Performance and Cost Analysis of a Structured Concrete Thermocline Thermal Energy Storage System, Master's thesis, University of Arkansas, 2012.
[27] Van Lew, J.T., Li, P.W., Chan, C.L., et al. Transient Heat Delivery and Storage Process in a Thermocline Heat Storage System, Proc. ASME IMECE 2009, November 13–19, Florida, USA.
[28] Strasser, M.N., Selvam, R.P. A Comparative Cost and Performance Analysis of Structured and Packed-Bed Thermocline Thermal Energy Storage Systems, Proc. ASME 2013 Heat Transfer Summer Conference, July 14–19, 2013, Minneapolis, MN, USA.
[29] Terrafore Technologies. http://www.terraforetechnologies.com/application-notes/terrakline/.
[30] G. Zanganeh, A. Pedretti, S. Zavattoni, et al., Packed-bed thermal storage for concentrated solar power – pilot-scale demonstration and industrial-scale design, Sol. Energy 86 (2012) 3084–3098.
[31] G. Zanganeh, A. Pedretti, S. Zavattoni, et al., Design of packed bed thermal energy storage systems for high-temperature industrial process heat, Appl. Energy 137 (2015) 812–822.
[32] A. Bejan, Convection Heat Transfer, John Wiley & Sons, Hoboken, New Jersey, 1984.
[33] S.M. Flueckiger, B.D. Iverson, S.V. Garimella, et al., System-level simulation of a solar power tower plant with thermocline thermal energy storage, Appl. Energy 113 (2014) 86–96.
[34] E. Votyakov, A. Bonanos, Algebraic model for thermocline thermal storage tank with filler material, Sol. Energy 122 (2015) 1154–1157.
[35] E.V. Votyakov, A.M. Bonanos, A perturbation model for stratified thermal energy storage tanks, Int. J. Heat Mass Transf. 75 (2014) 218–223.